Local structure of $Sr_2FeMo_xW_{1-x}O_6$ double perovskites across the composition-driven metal to insulator transition

2009 J. Phys.: Condens. Matter 21 195502

(http://iopscience.iop.org/0953-8984/21/19/195502)

J. Phys.: Condens. Matter **21** (2009) 195502 (9pp) doi:10.1088/0953-8984/21/19/195502

Local structure of $Sr_2FeMo_xW_{1-x}O_6$ double perovskites across the composition-driven metal to insulator transition

F Bardelli[1,2], C Meneghini[1,2], S Mobilio[1,2,3], Sugata Ray[4,5,6] and D D Sarma[5,6]

[1] CNR-TASC laboratory c/o GILDA-ESRF Grenoble, France, 6 Rue J Horowitz, 38043 Grenoble cedex 9, France
[2] Dipartimento di Fisica, Universita di 'Roma Tre', Via della Vasca Navale 84, I-00146 Rome, Italy
[3] INFN Laboratori Nazionali di Frascati, Via E Fermi 40, I-00044 Frascati (Rome), Italy
[4] Department of Materials Science, Indian Association for the Cultivation of Science, Jadavpur, Kolkata-700 032, India
[5] Centre for Advanced Materials, Indian Association for the Cultivation of Science, Jadavpur, Kolkata-700 032, India
[6] Solid State and Structural Chemistry Unit, Indian Institute of Science, Bangalore-560 012, India

E-mail: bardelli@esrf.fr

Received 28 January 2009, in final form 13 March 2009
Published 7 April 2009
Online at stacks.iop.org/JPhysCM/21/195502

Abstract

Sr_2FeMoO_6 oxides exhibit a half-metallic ferromagnetic (HM-FM) ground state and peculiar magnetic and magnetotransport properties, which are interesting for applications in the emerging field of spintronics and attractive for fundamental research in the field of heavily correlated electron systems. Sr_2FeWO_6 is an insulator with an antiferromagnetic (I-AFM) ground state. The solid solutions $Sr_2FeMo_xW_{1-x}O_6$ also have peculiar properties—W doping enhances chemical order which allows stabilization of the HM-FM state; as the W content exceeds a certain value a metal to insulator transition (MIT) occurs. The role of W in determining the physical properties of $Sr_2FeMo_xW_{1-x}O_6$ systems has been a matter of intense investigation. This work deals with the problem of the structural and electronic changes related to the MIT from a local perspective by means of x-ray absorption spectroscopy (XAS). This technique allows one to probe in detail the local structure and electronic modifications around selected absorber ions (W, Mo, Fe and Sr in our case). The results of XAS analysis in the whole composition range ($0 \leqslant x \leqslant 1$), in the near edge (XANES) and extended (EXAFS) regions, demonstrate an abrupt change of the local structure around the Fe and Mo sites at the critical composition, x_c. This change represents the microstructural counterpart associated with the MIT. Conversely, the local structure and electronic configuration of W ions remain unaltered in the whole composition range, suggesting indirect participation of W in the MIT.

1. Introduction

The Sr_2FeMoO_6 (SFM) and Sr_2FeWO_6 (SFW) compounds have a double perovskite structure and opposite magnetic and electronic transport properties: SFM is a half-metallic ferromagnet (HM-FM) with a high Curie temperature, while SFW is an antiferromagnetic insulator (I-AFM) at all temperatures. The magnetic and electronic transport properties of SFM have been thoroughly investigated [1–6]. Sarma *et al* [2, 3] proposed a novel mechanism to explain

the magnetic interaction between localized and conduction electrons, leading to a strong polarization of the mobile charge carriers. Further, the magnetic response and HM-FM state are strongly related to the relative arrangement of Fe and Mo ions on B and B′ sites (see figure 2) of the perovskite structure [1]: the regular alternation of Fe and Mo on the B and B′ sublattices (chemical order) enhances the Curie temperature and improves the magnetic response of the system [7]. $Sr_2FeMo_xW_{1-x}O_6$ (SFMW) solid solutions show interesting properties: W doping allows enhancement of the chemical order increasing the Curie temperature up to 450 K [8, 9]. However, as the W content exceeds $(1 - x_c) \sim 0.75$, $x_c \sim 0.25$ being the critical Mo concentration, a metal to insulator transition (MIT) occurs [7].

The role of W in determining the magnetic and electronic response of the solutions has been matter of wide investigation. Two models were proposed to explain the composition-driven MIT [10]: one based on a collective valence transition at x_c the other on a percolative mechanism.

In the first one, a collective oxidation state transition occurs at the critical concentration; in the high W content region ($x < x_c$) the oxidation state is Fe(II)–W(VI)/Mo(VI), the 5d conducting state of the Mo/W (B′) site is empty, and Fe(II) ions are antiferromagnetically coupled (as observed in SFW below 37 K). For $x \sim 0.25$, a valence transition (or valence fluctuation) takes place, changing the oxidation state of the ions into Fe(III)–W(V)/Mo(V); in this configuration, 5d Mo(V) derived states are occupied and the material becomes a conductor.

In the percolation scenario, the oxidation states of Mo and W remain 5+ and 6+, respectively, in the whole compositional range; every W(VI) doping in place of Mo(V) requires the transformation of a Fe(III) into Fe(II) to maintain the charge neutrality of the system. The system can be viewed as an inhomogeneous distribution of metallic ferrimagnetic SFM-like and insulating SFW-like domains. In this scenario the MIT is driven by the percolation of the system at the critical composition: for $x > x_c$, the system remains in the macroscopically HM-FM state (as in SFM), with a distribution of small, SFW-like, insulating and antiferromagnetic domains; for $x < x_c$, the insulating SFW-like regions grow in size, eventually engulfing the metallic SFM domains and giving rise to the observed MIT.

Accurate structural and electronic characterization as a function of the composition can give relevant information on the mechanisms underlying the origin of the MIT. Until now, structural characterizations have been mainly done using diffraction techniques (x-ray or neutron powder diffraction) [11–13]. These studies report an overall continuous cell expansion upon W substitution, accompanied by a smooth evolution of the lattice parameters.

It has to be noted that structural information obtained from diffraction concerns long range order properties of the lattice, which can be rather different from the short range ones (i.e. the local structure) that have a large influence on the physical properties of these compounds.

A preliminary XAS (x-ray absorption spectroscopy) study [14] on the SFMW solid solutions ($0 \leqslant x \leqslant 1$) has shown that changes at Fe and Mo near edge features (XANES) and at Fe–O and Mo–O nearest neighbor shells occur steeply at the MIT. These findings suggested the local structural behavior to be definitively different from the crystallographic one.

In this work we present a more accurate investigation of XAS data reported in [14], extending the analysis of the EXAFS (extended x-ray absorption fine structure) spectra up to the fourth coordination shell. This makes possible a direct comparison with crystallographic data, as the lattice parameter of the double perovskite cell corresponds to the fourth coordination shell. Experimental data confirmed sudden structure modifications across the MIT. The analysis of coordination shells higher than the first demonstrate that the structural rearrangement is not restricted to the nearest neighbors but also involves intermediate range order. Moreover, XAS data definitively confirm that the W ions preserve unaltered their local and electronic structure in the whole composition range, suggesting an indirect participation of W ions in the MIT.

2. Experimental details

2.1. Sample synthesis and characterization

Double perovskite SFMW solid solutions, with compositions $x = 0$, 0.05, 0.15, 0.2, 0.3, 0.6, 0.8 and 1, were prepared at the Indian Institute of Science of Bangalore, India. The SFM ($x = 1$) end compound was prepared using the optimized solid-state route described in detail in [15, 16]. The starting materials ($SrCO_3$, MoO_3 and Fe_2O_3) were mixed thoroughly and calcined at 900 °C in air for 3 h, then reduced in a flow of 10% H_2 in Ar at 1200 °C for 2 h. The other members of the SFMW series, with $x = 0.8$, 0.6, 0.3, 0.2, 0.15, 0.05 and 0, were prepared by the melt-quenching method under an Ar atmosphere exploiting the following reaction:

$$12\ SrCO_3 + 3\ Fe_2O_3 + x(5\ MoO_3 + Mo) + (1 - x)\ (5\ WO_3 + W) \longrightarrow 6\ Sr_2FeMo_xW_{1-x}O_6 + 12\ CO_2.$$

Synthesized compounds were annealed at 1300 °C for 6 h in an Ar atmosphere in order to achieve a homogeneous phase, which was probed by x-ray diffraction (XRD) to have no residuals from precursor phases. Homogeneous composition for different grains of each sample was tested by energy-dispersive analysis of x-rays (EDAX). Since the oxidation of the grain surfaces influences the transport properties, the samples were kept in a vacuum until the experiment and then measured, in a vacuum, at low temperature (77 K). The XRD analysis of the samples revealed a homogeneous single crystallographic phase, no impurities, and a high degree of chemical order. Doping with W rapidly enhances the chemical order, which increases from high (90–95%) in SFM to almost complete (100%) in SFW. The electrical resistivity as a function of temperature of all the investigated samples, reported in [7], clearly depicts two regimes: the first group, $x \geqslant 0.3$, presents lower resistivity and exhibits metallic behavior, while samples with compositions $x \leqslant 0.2$ are insulating. These results clearly established the MIT in the range $0.2 < x_c < 0.3$.

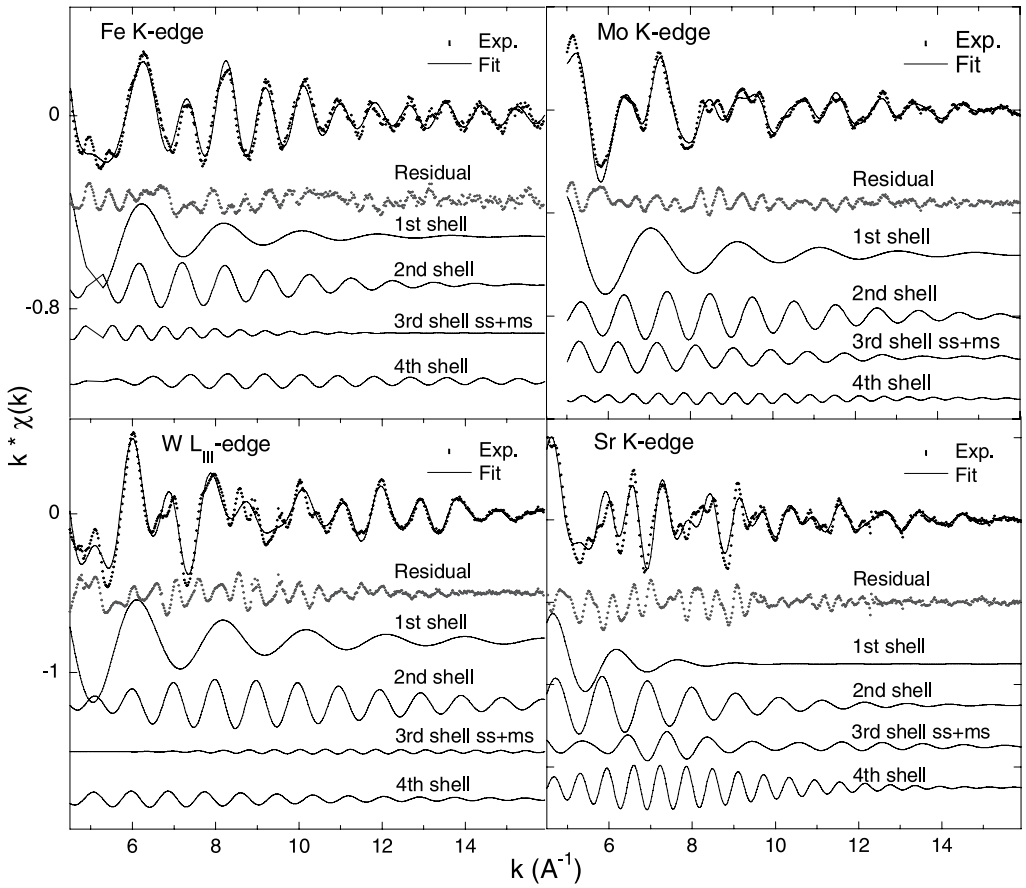

Figure 1. Examples of the EXAFS signals (points) and fits (lines) in the range 4.5–16 Å^{-1} for all of the investigated absorption edges. Also shown (shifted) are the residuals (gray points) and the contributions of the first four coordination shells (black lines) to the EXAFS signal: B(B′)–O, B(B′)–Sr, B′(B)–B(B′) and B(B′)–B(B′) (B = Fe, B′ = Mo(W)) and Sr–O, Sr–B(B′), Sr–Sr (pseudocube edge) and Sr–Sr′ (pseudocube face diagonal). Third shell single and multiple scattering paths (ss and ms) are reported as a single contribution. Since data were fitted in the k-space (without Fourier filtering), residuals contain a contribution from coordination shells higher than the first, which were not included in the fits.

2.2. XAS measurements and data analysis

XAS measurements were performed at the BM08 (GILDA) beamline [17] at the ESRF (Grenoble, France). Mo (20 000 eV), Fe (7112 eV), Sr (16 105 eV) K-edges and the W L_{III}-edge (10 207 eV) were investigated.

GILDA's monochromator uses two independent Si[311] crystals and a sagittal focusing system [17]. A pair of Pt/Pd mirrors is used for efficient harmonic rejection and vertical focussing of the x-ray beam.

All the XAS spectra were collected at liquid nitrogen temperature (77 K) in order to reduce the thermal contribution to the structural disorder and to avoid sample degradation. Samples for XAS measurements were prepared by grinding the sintered pellets in agate mortars; the finest powders were suspended in high purity ethanol and filtered by microporous membranes to deposit highly homogeneous thin films. Several films were piled up to obtain an optimal absorption for each investigated edge. This procedure allows one to obtain highly homogeneous samples, suitable for high quality XAFS data. XAS measurements were performed in transmission geometry measuring the x-ray intensity incident on the sample (I_0) and transmitted through it (I_T) by means of ionization chambers filled with a suitable gas type and pressure in order to have about 10% absorption for I_0 measurements and about 80% for I_T measurements. Raw absorption spectra are calculated as $\mu(E) = \ln(I_0/I_T)$. At least two spectra were collected for each absorption edge/sample and averaged for better statistics. Since the Mo content in the samples with $x = 0.05$ and 0.15 was too low to be measured in transmission geometry at the Mo K-edge, the Mo K fluorescence yield was measured using a high purity Ge detector. Due to technical drawbacks occurring with the fluorescence detector, the quality of spectra collected in the fluorescence mode is poorer than that of those collected in transmission mode.

Standard procedures have been adopted for data normalization, photoelectron edge energy definition (E_0) and extraction of the extended structural EXAFS signal $\chi(k)$ [18, 19]. Structural data refinement was performed by fitting the raw k^3-weighted EXAFS spectra (i.e. without Fourier filtering). The following (standard) expression for the theoretical signal was used:

$$\chi(k)_{\rm th} = S_0^2(k) \sum_j \frac{N_j}{kR^2} A_j(k) \sin[2kR_j + \phi_j(k)] \times \exp^{-2k^2\sigma_j^2} \exp^{-2R_j/\lambda_j(k)}$$

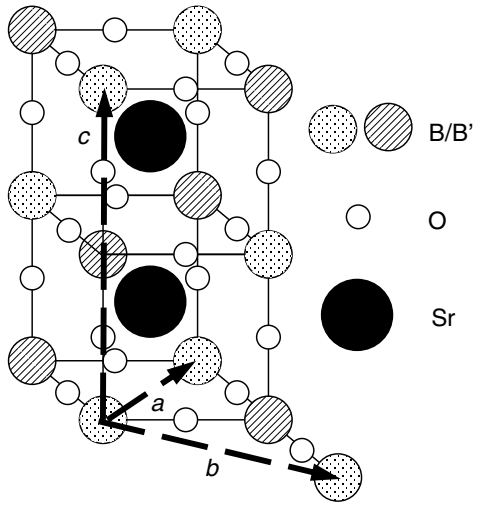

Figure 2. Double perovskite cell of a generic $A_2BB'O_6$ compound with the lattice parameters a, b and c shown (bold arrows). In our case A = Sr, B = Fe and B′ = Mo(W). Sr_2FeMoO_6 has tetragonal symmetry (space group $I4/m$, $a = b = 5.5685$ Å, $c = 7.9004$ Å, $\alpha = \beta = \gamma = 90°$) and Sr_2FeWO_6 belongs to the monoclinic group ($P2_1/n$, $a = 5.6508$ Å, $b = 5.6082$ Å, $c = 7.9252$ Å, $\alpha = \gamma = 90°$ and $\beta = 90.021°$).

where the sum runs over the main relevant neighboring shells, including single and multiple scattering contributions. A_j, ϕ_j and λ_j are the effective amplitude, phase and photoelectron mean free path functions. Atomic models calculated from crystallographic structures [20–22] using the ATOMS code [23] were used to obtain amplitude, phase and photoelectron mean free path functions exploiting the FEFF8.2 code [24, 25]. $S_0^2(k)$ is an empirical parameter taking into account the many-body losses.

Contributions to the overall EXAFS signal to be used in the refinement were chosen via a trial and error procedure applying a F-test to exclude the statistical significance of the weaker ones. Figure 1 shows examples of experimental EXAFS signals, best fit curves and partial contributions from the first four coordination shells used in the analysis. The high quality of the EXAFS spectra permitted a reliable refinement in the range 4.5 $Å^{-1} \leqslant k \leqslant 16$ $Å^{-1}$ exploiting a data refinement program (FITEXA) based on the MINUIT package developed at CERN [26]. For the jth shell contribution to the EXAFS signal the refinable structural parameters were the multiplicity number (N_j), the effective photoelectron path length (R_j) and the Debye–Waller factor (σ_j^2). The coordination numbers were kept fixed to the values derived by the crystallographic models and S_0^2 was fixed to values derived from first shell refinements. Therefore, a maximum of two parameters (R_j and σ_j^2) were refined for each shell. Geometrical constraints were applied to single and multiple scattering photoelectron path lengths (in particular for the third coordination shell) in order to reduce the free parameters in the fitting step. An additional parameter, the correction to the photoelectron energy scale (E_0, the same for all shells), was refined. Statistical uncertainties on the parameters have been calculated using the MINOS subroutine from the MINUIT package, which takes into account correlations between refined parameters [26].

Refinements of Fe and Mo K-edges and the W L_{III}-edge XAS data involved the following contributions:
1st shell: A–O (A being the absorber: Fe, Mo, or W), at a distance of about 2 Å.
2nd shell: A–Sr, around 3.41 Å.
3rd shell: A–O–B (B = Fe or Mo/W) around 3.96 Å (perovskite pseudocube edge), which include the single (A–B) and multiple scattering paths involving both B and O atoms.
4th shell: A–B at ∼5.57 Å (pseudocube face diagonal).

Modeling the third shell is a non-trivial issue since we are dealing with a doped compound: in the case of perfect chemical order (no antisite defects) the Fe absorber would 'see' both W and Mo as back-scatterers, while Mo and W only see Fe. Therefore, to refine the Fe edge we used both Fe–Mo and Fe–W contributions weighted according to the sample composition x. Further, we verified that Fe–Fe third shell contributions were negligible.

Refining Mo and W edges, only Mo–Fe and W–Fe contributions were used (for the Mo and W edges, respectively), as we found Mo–W(Mo) and W–Mo(W) signals to be negligible. Notice that, owing the large differences of amplitude and phase functions of Fe, Mo and W, the sensitivity to the different contributions is high.

The lower quality of Mo K-edge spectra, measured in fluorescence mode, for $x = 0.05$ and 0.15 samples only allowed refinement of the Mo–O nearest neighbor shell.

The local structure around Sr ions, being at the center of the perovskite pseudocube unit, is different from that of Fe, Mo and W and includes the following contributions:
1st shell: Sr–O, at a distance around 2.6–2.7 Å.
2nd shell: Sr–B (B = Fe, Mo, or W), around 3.41 Å.
3rd shell: Sr–Sr, at about 3.96 Å (perovskite pseudocube edge).

The Sr–Sr 4th shell, Sr–Sr (pseudocube face diagonal), which is a multiple scattering path involving Sr and O.

Contemporary refinement of local structure around the different absorbers provided further constraints on the structural parameters.

3. Results

3.1. XANES

The near edge absorption spectra of all the measured edges and samples are reported in figure 3. At first sight, XANES spectra reveal clear differences among data collected at Sr K-edges and W L_{III}-edges and those measured at Fe and Mo K-edges. In fact no relevant changes can be observed at the W L_{III}-edge in the whole concentration range, either in the spectral features or in the edge energy position (figure 3, panel (c)). Also the Sr K-edge XANES (figure 3, panel (d)) depict only weak modifications as a function of composition: in the $x < 0.3$ composition region the white line is slightly broader and the spectral features appears smoother. The lack of relevant modifications on W and Sr XANES indicates minor changes in the local environment of these ions across the MIT. Conversely, XANES spectra of Mo and Fe K-edges (figure 3, panels a and b) clearly depict a bimodal trend with an abrupt discontinuity of the spectral features at the critical

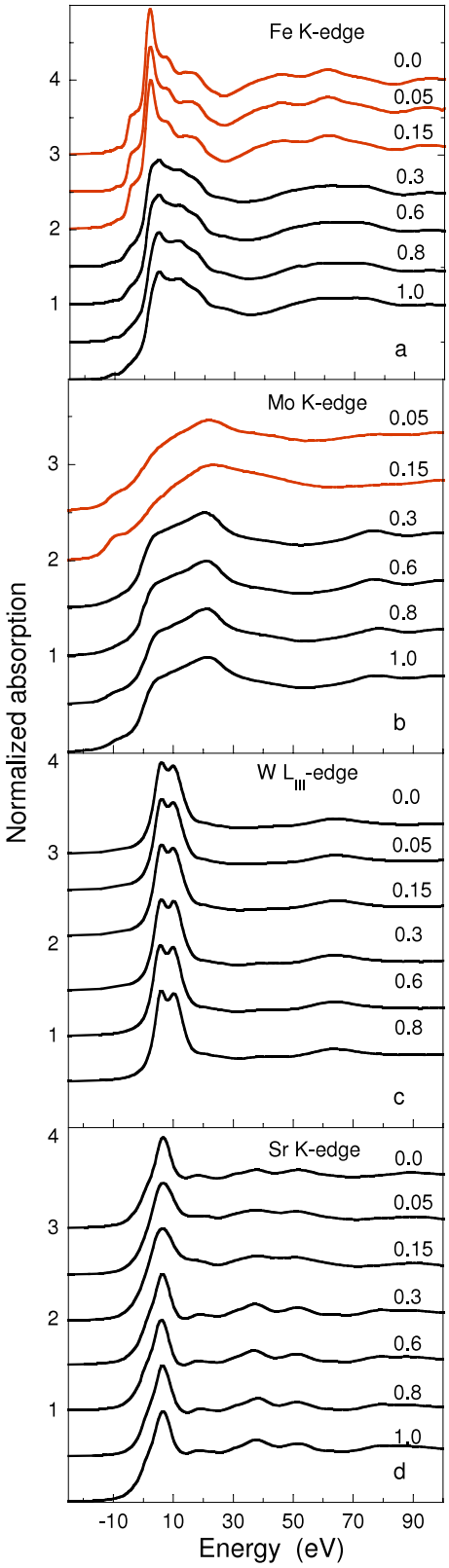

Figure 3. XANES region of the pre-edge subtracted and normalized XAS spectra of all the samples at the investigated absorption edges. Step-like changes as a function of the composition x at the Fe (a) and Mo (b) edges are evident. Conversely, spectra at W (c) and Sr (d) edges show little or no change.

(This figure is in colour only in the electronic version)

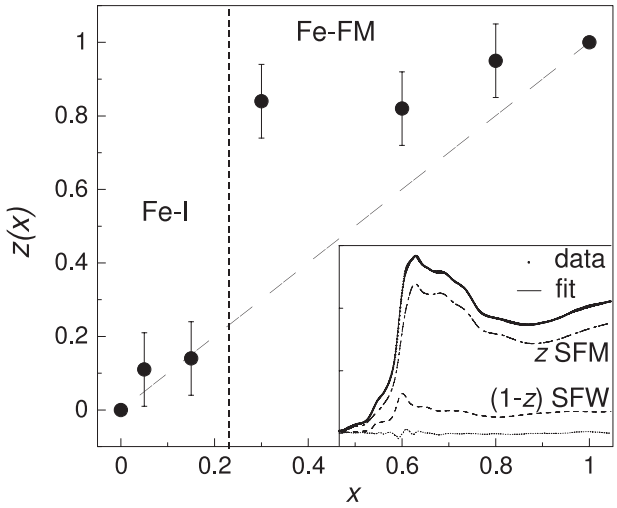

Figure 4. Values of the weight parameter z for the linear combination, $\mu(x) = z\mu_{\mathrm{SFM}} + (1-z)\mu_{\mathrm{SFW}}$ of end compounds (SFM and SFW) at the Fe K-edge. The inset reports the experimental absorption spectrum for the $x = 0.3$ sample together with the fit, the residual and the fractions of the end compounds, as an example.

concentration. Furthermore, all Mo and Fe spectra of samples with $x > x_c$ closely resemble that of the $x = 1$ (SFM) sample, while all spectra of samples with $x < x_c$ closely resemble that of the $x = 0$ (SFW) sample.

As shown in the inset of figure 4, the XANES features of intermediate compounds, $\mu(x)$, at the Fe K-edge can be remarkably well reproduced using a linear combination of the spectra of the end compounds μ_{SFM}, $x = 1$, and μ_{SFW}, $x = 0$:

$$\mu(x) = z\mu_{\mathrm{SFM}} + (1-z)\mu_{\mathrm{SFW}}. \tag{3.1}$$

Least square minimization has been performed using the XPSFIT code [27], based on the MINUIT libraries. In $z = 1$ (SFM) and $z = 0$ (SFW), Fe ions are in two distinct states: the ferromagnetic metallic state (Fe-FM) and the insulating state (Fe-I), respectively. Results of the fitting show that, in intermediate compounds, the Fe average configuration arises from the contribution of two extreme situations, with z representing the fraction of Fe ions in the FM state. The fraction of Fe-I and Fe-FM changes steeply across x_c, demonstrating that, in the metallic phase ($x > x_c$), the largest fraction of Fe ions retains the same structural/electronic state of pure SFM (for sample with $x = 0.3$, more than 80% of the Fe ions are in the Fe-FM state). In the insulating phase ($x < x_c$) the fraction of Fe-I and Fe-FM ions appears to follow nominal sample composition (x) within the experimental error bars. XANES features of the Mo K-edge also depict abrupt changes, presenting a pre-edge shoulder for $x < x_c$ (insulating phase) that suddenly disappears for $x_c < x$ (metallic phase).

3.2. EXAFS

Quantitative structural parameters derived from the analysis of the EXAFS spectra are reported in tables 1–4 and interatomic distances are summarized in figure 5 for convenience.

Table 1. First shell bond distances (R) and Debye–Waller factors (σ^2) for the Fe, W, Mo and Sr absorber atoms. Numbers in parentheses represent the error bars on the last digit. The error bars on σ^2 have been estimated taking into account the correlations among all the parameters and are between 20 and 60 at.%.

	Fe–O		W–O		Mo–O		Sr–O	
x	R (Å)	σ^2 (10^{-3} Å^2)	R (Å)	σ^2 (10^{-3} Å^2)	R (Å)	σ^2 (10^{-3} Å^2)	R (Å)	σ^2 (10^{-3} Å^2)
1.0	2.00(2)	4			1.94(1)	3	2.65(2)	10
0.8	2.01(2)	7	1.91(1)	2	1.94(1)	3	2.64(2)	11
0.6	2.02(1)	5	1.91(1)	2	1.94(1)	3	2.64(2)	10
0.3	2.03(1)	6	1.91(1)	2	1.95(1)	2	2.65(2)	10
0.15	2.11(1)	4	1.92(1)	1	1.90(2)	2	2.58(2)	13
0.05	2.08(1)	4	1.91(1)	3	1.89(2)	2	2.59(2)	12
0.0	2.09(1)	2	1.91(1)	2			2.60(2)	13

Table 2. Second shell bond distances (R) and Debye–Waller factors (σ^2) for the absorber atoms Fe, W and Mo. Numbers in parentheses represent the error bars on the last digit. The error bars on σ^2 have been estimated taking into account for the correlations among all the parameters and are between 20 and 60 at.%.

	Fe–Sr		W–Sr		Mo–Sr	
x	R (Å)	σ^2 (10^{-3} Å^2)	R (Å)	σ^2 (10^{-3} Å^2)	R (Å)	σ^2 (10^{-3} Å^2)
1.0	3.41(1)	8			3.43(1)	3
0.8	3.42(2)	8	3.45(1)	4	3.43(1)	3
0.6	3.42(1)	5	3.44(1)	3	3.42(1)	3
0.3	3.43(1)	6	3.45(1)	4	3.41(1)	2
0.15	3.50(1)	6	3.46(1)	7	—	2
0.05	3.51(1)	6	3.44(1)	7	—	2
0.0	3.49(1)	6	3.45(1)	6		

The global evolution of structural parameters as a function of sample composition closely resembles the trend observed for the XANES regions: a large (up to 0.1 Å) and abrupt rearrangement of the microstructure as a function of the composition occurs crossing the critical concentration x_c. For Mo content decreasing down to $x = 0.3$, the local structure of the samples remains similar to that of the SFM (HM-FM) end compound, while below $x = 0.3$ the local structure suddenly rearranges to that of the SFW (I-AFM). The analogy with XANES results is particularly evident at the nearest neighbor shells (figure 5): Fe–O and Mo–O bond lengths change abruptly, and in opposite ways, crossing x_c: Fe–O bonds increase by about 0.1 Å and Mo–O decrease by about 0.05 Å. Conversely, W–O bonds remain stable at about 1.91 Å over the whole compositional range. Longer Fe–O bonds are observed in W-rich compounds ($x < 0.3$), in agreement with the hypothesis of a lower oxidation state of Fe in the insulating phase (the Fe(II)–O bond in FeO oxide is 2.15 Å). On the other hand, the shorter Fe–O distance in the HM-FM phase suggests a higher Fe oxidation state (average Fe(III)–O distance in Fe_2O_3 is about 2.02 Å).[7] Finally, the observed average Sr bonds undergo a contraction of about 0.05 Å below $x = 0.3$, as a consequence of the expansion of the FeO_6 octahedra.

In the second shell (B/B′–Sr distances, B = Fe, B′ = Mo/W), the W–Sr bonds remain unchanged in the whole concentration range, while the Fe–Sr ones increase abruptly. No reliable information about Sr–Mo and Mo–Sr bonds is available due to the lower quality of the low Mo concentration ($x = 0.05$ and 0.15) spectra.

The structural changes observed in the third and fourth shell show an overall structural rearrangement, consistent with the unit cell expansion observed in diffraction studies [12, 11, 13] but retaining a enhanced, step-like, change at the Fe edge and Mo edges, especially for the first two coordination shells.

The Debye–Waller factors (σ^2) do not show a relevant trend as a function of composition, except for the Fe–O bonds which have higher σ^2 in the SFM (σ^2_{FeO} 4×10^{-3} Å^2) than in the SFW (σ^2_{FeO} 2×10^{-3} Å^2) end compound. This finding is again in agreement with the hypothesis of a Fe(III)-like and Fe(II)-like environment in $x = 1$ and $x = 0$ compounds, respectively. Debye–Waller factors belonging to the first coordination shell of intermediate compounds are larger than in the extreme compounds, indicating a more disordered local environment. It is worth noting that we found a strong correlation among the Debye–Waller (σ^2) parameters, which becomes progressively larger for longer distances. This gives large error bars which can only be estimated looking at the correlation matrices given by MINUIT. Notice, however, that the correlation among Debye–Waller and bond distances remains small (less than 10–20%), so having less affect on the interatomic distances, which are the most relevant parameters for our discussion.

These findings suggest that the rearrangement of the local structure observed at the critical concentration is related to the localization of the charge carriers on the Fe sites in the insulating phase, resulting in a lower oxidation state, in agreement with the theory.

4. Discussion

We can summarize the results obtained in the following points:

(a) XANES features do not (or only weakly) change at the W and Sr edges. Conversely, crossing the critical concentration x_c, abrupt changes are observed at the Mo and Fe edges.

(b) XANES data for Mo-rich ($x_c < x < 1$) and W-rich ($0 < x < x_c$) samples closely resemble those for the end compounds $x = 1$ and $x = 0$, respectively.

[7] Fe(III) ions in Fe_2O_3 are bonded to six oxygens in a distorted octahedral configuration: three Fe–O neighbors at 1.94 Å and three at 2.11 Å.

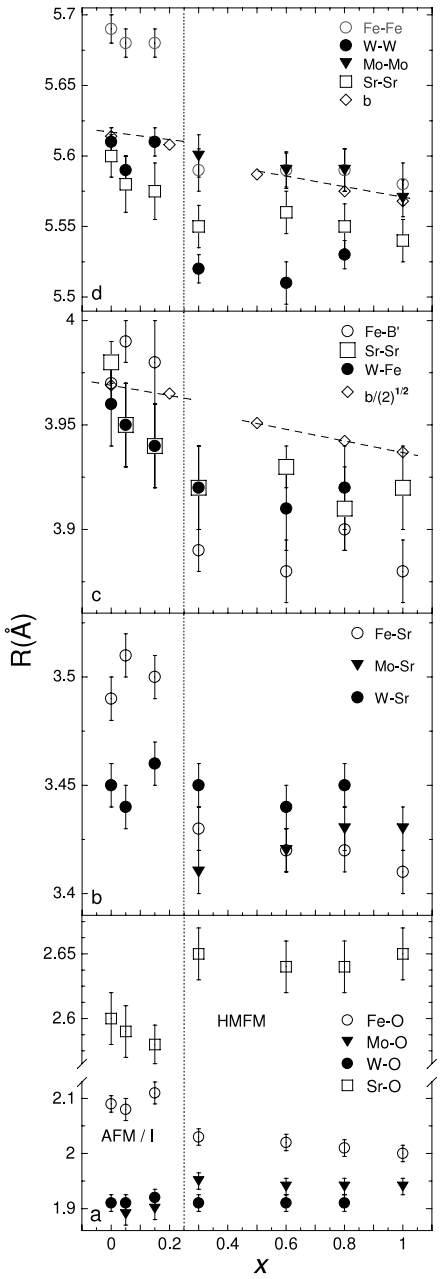

Figure 5. Evolution of the local structure across the MIT around the investigated absorbers. Panel (a) shows the abrupt and opposite change of the Fe–O and Mo–O nearest neighbor coordination shells compared to the smooth trend of W–O shell crossing the critical composition $x_c \sim 0.25$. Sr–O bonds rearrange reflecting the expansion of the FeO_6 octahedra in the insulating phase. Panel (b): in the second shell, corresponding to half of the pseudocube diagonal length, W–Sr distances do not change over the whole concentration range, while Fe–Sr changes abruptly at x_c. Panel (c): in the third shell (corresponding to the length of the pseudocube edge) the Fe–B′ (B′ = Mo/W) distance changes steeply at x_c while Sr–Sr and W–Fe increase smoothly, increasing the W content. The trend of the crystallographic parameter $b/\sqrt{2}$ from neutron powder diffraction [11] is also reported for a ready comparison with XAS data (points connected by a broken line). Panel (d): the fourth shell (corresponding to the length of the pseudocube face diagonal) shows a sudden increase of W–W and Fe–Fe distances crossing x_c that resembles the evolution of lattice parameter b obtained from neutron powder diffraction data [11] (points connected by a broken line). No data are available at the Mo edge below x_c for shells higher than the first.

(c) The analysis of the Fe XANES spectra shows that, in the $x > x_c$ region, the fraction of Fe ions in the SFM-like (Fe-FM) structural and electronic configuration remains almost constant (∼80%) down to the critical composition x_c. Conversely, below x_c almost all the Fe ions revert to the SFW-like (Fe-I) configuration.

(d) Matching XANES results, the structural parameters obtained from quantitative refinement of the EXAFS spectra at Fe and Mo K-edges reveal abrupt discontinuities crossing x_c. Conversely, the W and Sr local environment follows a smoother evolution similar to that reported from diffraction studies [12, 11, 13] and the structural rearrangements mainly occur at a local atomic scale around Sr as a consequence of expansion of FeO_6 octahedra.

(e) Fe–O bond distances are compatible with Fe in a lower oxidation state for $x < x_c$ (W rich, I-AFM phase), and with Fe in higher oxidation state for $x > x_c$ (Mo rich, HM-FM phase).

XAS results tend to rule out the valence transition scenario [10], which would involve a valence change of W ions from 6+ in the I-AFM ($x < x_c$) to 5+ in the HM-FM phase ($x_c < x$). Our finding are in agreement with recent XPS measurements [28] showing that W ions do not change their electronic structures and oxidation states as a function of the composition. At least from a structural point of view, our results do not match the phase separation in SFM-like (HM-FM) and SFW-like (I-AFM) clusters implied in the original formulation of the percolative transition model. As a matter of fact, such a model would imply the size of I-AFM and HM-FM domains to change according to the nominal Mo concentration x. If this was the case, the weight parameter z in equation (3.1) would follow a linear trend reflecting the nominal composition of the samples ($z \sim x$), in contrast with our findings. Nevertheless, a phase separation could still not be excluded for $x < x_c$ (see figure 4). On the basis of these results we suggest the percolative model to be the more appropriate to describe the observed MIT but we propose a small modification to the original version, which dismisses the hypothesis of phase separation (at least in the metallic phase).

In the I-AFM phase ($x < x_c$) all charge carriers are localized, so that Fe ions remain in the SFW-like state (Fe-I). The addition of Mo ions increases Fe–Mo coupling and, as the percolative concentration of Mo ions is reached, the conduction band formed by Fe–Mo hybridized states grows in width, allowing almost complete charge carrier delocalization. Such delocalization involves a large fraction (about 80%) of Fe sites even at $x = 0.3$. The role of W in this model appears to be indirect, as no changes are observed in its local structure or electronic configuration in the whole compositional range. The effect of W doping on the MIT seems limited to the reduction of the Fe–Mo conduction bandwidth. From the structural point of view, the entire rearrangement of the local structure at the critical composition is driven by the localization of the charge carriers on the Fe sites, which become prevalently 2+, Fe(II) having a larger ionic radius (0.78 Å for Fe(II), 0.64 Å for Fe(III)).

Table 3. Third shell bond distances (R) and Debye–Waller factors (σ^2) for the absorber atoms Fe, W, Mo and Sr (B′ = Mo(W)). Numbers in parentheses represent the error bars on the last digit. The error bars on σ^2 have been estimated taking into account the correlations among all the parameters and are between 20 and 60 at.%.

	Fe–B′		W–Fe		Mo–Fe		Sr–Sr	
x	R (Å)	σ^2 (10^{-3} Å^2)	R (Å)	σ^2 (10^{-3} Å^2)	R (Å)	σ^2 (10^{-3} Å^2)	R (Å)	σ^2 (10^{-3} Å^2)
1.0	3.88(1)	8			3.92(2)	1	3.92(2)	9
0.8	3.90(1)	6	3.92(2)	3	3.89(1)	2	3.91(2)	9
0.6	3.88(1)	8	3.89(2)	2	3.92(1)	1	3.93(1)	7
0.3	3.89(1)	16	3.93(2)	6	3.90(2)	2	3.92(2)	8
0.15	3.98(1)	13	3.92(5)	3	—	—	3.94(4)	7
0.05	4.00(1)	13	3.95(4)	6	—	—	3.95(4)	5
0.0	3.97(4)	15	3.96(3)	4			3.98(1)	6

Table 4. Fourth shell bond distances (R) and Debye–Waller factors (σ^2) for the absorber atoms Fe, W, Mo and Sr. Numbers in parentheses represent the error bars on the last digit. The error bars on σ^2 have been estimated taking into account the correlations among all the parameters and are between 20 and 60 at.%.

	Fe–Fe		W–W		Mo–Mo		Sr–Sr	
x	R (Å)	σ^2 (10^{-3} Å^2)	R (Å)	σ^2 (10^{-3} Å^2)	R (Å)	σ^2 (10^{-3} Å^2)	R (Å)	σ^2 (10^{-3} Å^2)
1.0	5.58(3)	11			5.57(2)	7	5.54(2)	10
0.8	5.59(2)	2	5.53(1)	6	5.59(3)	10	5.55(3)	10
0.6	5.59(2)	6	5.51(2)	5	5.59(3)	10	5.56(2)	10
0.3	5.59(2)	7	5.52(2)	8	5.60(5)	12	5.55(2)	6
0.15	5.68(1)	2	5.61(1)	12	—	—	5.56(3)	7
0.05	5.68(1)	2	5.59(1)	5	—	—	5.57(3)	5
0.0	5.69(1)	3	5.61(1)	6			5.61(2)	8

It is interesting to compare the local structure derived from our XAS results to the crystallographic information derived from diffraction techniques. In figure 5, panels c and d, the lattice parameters b (pseudocube face diagonal) and $b/\sqrt{2}$ (pseudocube edge) from [11] are reported. A discontinuity in b and $b/\sqrt{2}$ versus x can only be supposed, so that only the possibility of comparing long range order (diffraction) and local order (XAS) allows a definitive assessment of the step-like nature of the structural transition. Our findings suggest that interpretation of diffraction data from previous studies should be revised in terms of a more abrupt structural change on a local scale.

5. Conclusions

We performed accurate XAS investigations on $Sr_2FeMo_xW_{1-x}O_6$ solid solutions highlighting a peculiar trend of the local atomic structure as a function of composition. This behavior is closely related to the composition-driven MIT in these compounds. Crossing the critical composition, sudden structural changes are clearly observed at the Fe and Mo K-edge XAS spectra, both in the near edge (XANES) and extended (EXAFS) regions of the absorption spectra. The absence of significant changes as a function of composition in W L_{III}-edge XAS spectra allows us to exclude a direct role for W ions in the MIT (rather than stated in the valence transition model [10]), while the modifications observed at the Fe and Mo K-edges represent the microstructural counterpart of the MIT. The results of the present work suggest the percolative model [10] to be the more appropriate to describe the MIT. Nevertheless, according to our findings, we propose a modified version of this model, dismissing, at least in the metallic phase, the hypothesis of phase separation in SFM-like and SFW-like clusters.

Adding W reduces the width of the Fe–Mo conduction band, while the charge neutrality of the system is maintained by the transformation of a Fe(III) ion in Fe(II) for each W(VI) in place of Mo(V). This implies that Mo and W do not change their oxidation state in the whole compositional range. When the percolation composition (x_c) is reached, charge carriers suddenly localize on Fe sites due to the disruption of the Fe–Mo conduction band. The system becomes insulating and stabilizes in a SFW-like structural and electronic configuration. The observed rearrangement of the local structure at the critical concentration is thus the fingerprint of charge localization on the Fe sites.

The abrupt local structure modifications observed by XAS are an original finding in contrast with the continuous, smoother trend suggested by diffraction studies [11–13] on the same compounds.

Acknowledgments

This research has been supported by the ‘Consiglio Nazionale delle Ricerche-Istituto Nazionale per la Fisica della Materia (CNR-INFM)’ and the University of ‘Roma Tre’. We would like to thank the staff of the Italian beamline at the European Synchrotron Radiation Facility at Grenoble (GILDA-BM08), F D’Acapito, C Maurizio, M Rovezzi, F D’Anca, V Tullio, V Sciarra and F Campolungo.

References

[1] Sarma D D, Sampathkumaran E V, Ray S, Nagarajan R, Majumdar S, Kumar A, Nalini G and Guru Row T N 2000 *Solid State Commun.* **114** 465–8
[2] Sarma D D 2001 *Curr. Opin. Solid State Mater. Sci.* **5** 261
[3] Sarma D D, Mahadevan P, Saha-Dasgupta T, Ray S and Kumar A 2000 *Phys. Rev. Lett.* **85** 2549
[4] Balcells Ll, Navarro J, Bibes M, Roig A, Martinez B and Fontcuberta J 2001 *Appl. Phys. Lett.* **78** 781
[5] Niebieskikwiat D, Sanchez R D, Caneiro A, Morales L, Vasquez-Mansilla M, Rivadulla F and Hueso L E 2000 *Phys. Rev.* B **62** 3340
[6] Chmaissem O, Kruk R, Dabrowski B, Brown D E, Xiong X, Kolesnik S, Jorgensen J D and Kimball C W 2000 *Phys. Rev.* B **62** 14197
[7] Ray S, Kumar A, Majumdar S, Sampathkumaran E V and Sarma D D 2001 *J. Phys.: Condens. Matter* **13** 607
[8] Ward R and Longo J 1961 *J. Am. Chem. Soc.* **83** 2816
[9] Patterson F K, Moeller C W and Ward R 1963 *Inorg. Chem.* **2** 196
[10] Kobayashi K I, Okuda T, Tomioka Y, Kimura T and Tokura Y 2000 *J. Magn. Magn. Mater.* **218** 17
[11] Sanchez D, Alonso J A, Garcia-Hernandez M, Nartinez-Lope M J and Casais M T 2005 *J. Phys.: Condens. Matter* **17** 3673
[12] Douvalis A P, Venkatesan M, Coey J M D, Grafoute M, Greneche J-M and Sryanaraynan R 2002 *J. Phys.: Condens. Matter* **14** 12611
[13] Dass R I and Goodenough J B 2001 *Phys. Rev.* B **63** 64417
[14] Bardelli F, Meneghini C, Mobilio S, Ray S and Sarma D D 2006 *Mater. Sci. Eng.* B **126** 226
[15] Kimura T, Sawada H and Terakura K 1998 *Nature* **395** 677
[16] Nagakawa T 1968 *J. Phys. Soc. Japan* **24** 806
[17] Pascarelli S, Bosherini F, D'Acapito F, Hrdy J, Meneghini C and Mobilio S 1996 *J. Synchrotron Radiat.* **3** 147
[18] Klementev K V 2001 *J. Phys. D: Appl. Phys.* **34** 209
[19] Vlaic G, Andreatta D, Cepparo A, Colavita P E, Fonda E and Michalowicz A 1999 *J. Synchrotron Radiat.* **6** 225
[20] Arulraj A, Ramesha K, Gopalakrishnan J and Rao C N R 2000 *J. Solid State Chem.* **155** 233
[21] Kim S B and Kim C S 2001 *Sae Mulli* **43** 341
[22] Fu Z and Li W 1995 **38** 309
[23] Ravel B 2001 *J. Synchrotron Radiat.* **8** 314
[24] Ankudinov A L, Ravel B, Rehr J J and Conradson S D 1998 *Phys. Rev.* B **58** 7565
[25] Rehr J J and Albers R C 2000 *Rev. Mod. Phys.* **72** 621
[26] James F and Winkler M 2004 Cern http://www.cern.ch/minuit
[27] Meneghini C http://webusers.fis.uniroma3.it/∼meneghini/software.html
[28] Ray S *et al* unpublished